Simulation of Reinforced Concrete Structure under Impact Loading using Meshfree Cohesive Failure Approach

H. S. Lu[1], J. Y. Zhao[1] , X. W. Wang[2]，X. Lei[2],
C. T. Wu[3] , and Y. C. Wu[4]

[1]*Shanghai Hengstar Technology Co., Ltd. Shanghai 201203,P.R.China*
[2] *Shanghai Nuclear Engineering Research and Design Institute, Shanghai 200233, P. R. China*
[3]*Livermore Software Technology Corporation (LSTC), Livermore, CA 94551,USA*
[4]*Karagozian & Case, Burbank, CA 91505,USA*

Abstract

Reliable numerical simulation of failure is important for the design and planning of new solids and structures, as well as for the safety assessment of existing ones. In the past two decades, gradient and non-local models for regularizing loss of ellipticity due to material failure using non-standard finite element method and more recently the meshfree method have been the topic of considerable research. Alternatively, discontinuous partition of unity enrichments and meshfree visibility concepts were proposed and used in finite element method (also called extended finite element method - XFEM) and meshfree method to model cracks.

Due to the fact that the description of crack plane in XFEM using level set method still presents several difficulties in the three-dimensional simulation of solids, the meshfree method using visibility concept is tested for the solid failure analysis of reinforced concrete structure under impact loading. The current method incorporates the discontinuous field into the generalized meshfree approximation [1] by the introduction of visibility approach [2]. To determine the onset of fracture and subsequently the crack propagation, a stress-based initial-rigid cohesive cracking model was developed for the brittle and semi-brittle materials. After the insertion of new crack, the state variables are interpolated and transferred to the new stress point using second-order meshfree approximation [3]. To integrate the discrete equations involving the crack plane, the strain smoothing algorithm developed in SCNI method [4] was adopted in this development. A typical reinforced concrete structure under impact loading failure involving multi-cracks is modeled using the developed method and results are presented.

Generalized Meshfree Approximation

The generalized meshfree (GMF) approximation method can be used to construct a convex, non-convex, or combined convex and non-convex approximation for meshfree computation. The GMF approximation has one unique feature. That is it naturally bears the weak Kronecker-delta property at boundaries regardless of its convexity or non-convexity. This property makes the imposition of essential boundary conditions in meshfree methods easier. The first-order GMF approximation in one dimension is described as follows:

$$\Psi_i(x,\lambda) = \frac{\psi_i}{\psi} = \frac{\phi_a(x;X_i)\Gamma_i(X_i,\lambda)}{\sum_{j=1}^{n}\phi_a(x;X_j)\Gamma_j(X_j,\lambda)} \quad \text{for fixed } x, \tag{1}$$

subjected to

$$R(x) = \sum_{i=1}^{n}\Psi_i X_i = 0 \quad \text{(linear constraints)}, \tag{2}$$

where

$$\psi_i = \phi_a(x;X_i)\Gamma_i(X_i,\lambda), \tag{3}$$

$$\psi = \sum_{i=1}^{n}\psi_i = \sum_{i=1}^{n}\phi_a(x;X_i)\Gamma_i(X_i,\lambda). \tag{4}$$

In the GMF approximation, the property of the partition of unity is automatically satisfied by the normalization in Eq. (1). The completion of the GMF approximation is achieved by finding λ to satisfy Eq. (2). To determine λ at any fixed x in Eq. (1), a root-finding algorithm is required for the non-linear base functions.

The spatial derivative of the GMF approximation is given by

$$\frac{d\Psi_i}{dx} = \Psi_{i,x} + \Psi_{i,\lambda}\lambda_{,x}, \tag{5}$$

where $\quad \Psi_{i,x} = \dfrac{\psi_{i,x}}{\psi} - \Psi_i\sum_{j=1}^{n}\dfrac{\psi_{j,x}}{\psi},$ (6)

$$\psi_{i,x} = \phi_{a,x}\Gamma_i + \phi_a\Gamma_{i,x}, \tag{7}$$

$$\Psi_{i,\lambda} = \frac{\phi_a\Gamma_{i,\lambda}}{\psi} - \Psi_i\sum_{j=1}^{n}\frac{\phi_a\Gamma_{j,\lambda}}{\psi}, \tag{8}$$

$$\lambda_{,x} = -J^{-1}R_{,x}, \tag{9}$$

$$J = \sum_{i=1}^{n}\frac{\phi_a\Gamma_{i,\lambda}}{\psi}X_i - R\sum_{j=1}^{n}\frac{\phi_a\Gamma_{j,\lambda}}{\psi}, \tag{10}$$

$$R_{,x} = \sum_{i=1}^{n}\Psi_{i,x}X_i + 1. \tag{11}$$

By choosing appropriate basis functions in the GMF approximation, some well-known convex or non-convex approximations, such as Shephard, Moving-least-squared (MLS), Reproducing kernel (RK) and Maximum entropy (ME) approximations, can be recovered. When the basis function is non-positive such as polynomials, the convex approximation property and Kronecker-delta property at the boundaries are lost and a boundary correction function [1] has to be introduced to achieve the local convexity at the boundary nodes. The MLS and RK approximations are the typical non-convex approximations.

In the MLS or the RK approximation, polynomial basis functions are introduced to meet the polynomial reproducing conditions. As in the ME approximation, the employment of exponential basis function takes into account the exponential distribution of the probability at the node in the view point of the information theory. Therefore it yields a convexity in the approximation since the exponential function is non-negative. It is noted that other probability density function can

also be chosen as a basis function and different entropy measure can also be used to obtain the convex approximation. The enriched basis function and weight function play an important role in controlling the smoothness and convexity of the approximation. The coefficient λ in Eq. (1) can be viewed as a corrected weight to impose polynomial reproducibility.

Table 1 gives the typical basis functions used to generate the convex and non-convex GMF approximations. In this study, the GMF(tanh) approximation is adopted for the simulation.

Table 1. Examples of basis functions in the GMF approximations

Convexity	Basis function	Abbreviation	Note
Convex approximation	e^x	GMF(*exp*)	ME Approximation (Shannon entropy)
	$1+tanh(x)$	GMF(*tanh*)	New approximation
	$1+\dfrac{2}{\pi}tan^{-1}(x)$	GMF(*atan*)	New approximation
Non-convex approximation	$\left(1+\dfrac{1-\alpha}{\alpha}x\right)^{\frac{1}{\alpha-1}}$ (Renyi basis function)	GMF(*Renyi*)	ME Approximation (Renyi entropy) $(0.5<\alpha<1.0)$
			MLS approximation $(\alpha=2)$
	$1+x$	GMF(*MLS*)	MLS approximation
	$1+x^3$	GMF(x^3)	New approximation
	$e^x(1+x^3)$	GMF(exp·x^3)	New approximation

Review of K&C Concrete Model (*MAT_72）

The Release III KCC model was made available in LS-DYNA in 2004. The model has been extensively verified in both dynamic and quasi – static load environments [5, 6, 7]. To verify the basic capabilities of the KCC model, several single element numerical results are included herein.
Figure 1 shows the stress – strain relationship for a single element UUC test. It is seen that a yield point is reached first, then very limited hardening undergoes, and finally, strain softening phenomenon is observed. It should be pointed out that, in the Figure, positive volumetric strain corresponds to volume compaction and negative volumetric strain corresponds to volume expansion. As a consequence, it can be concluded that the shear dilation effect is captured by the material model properly, since the concrete is compacted early on and after it reaches its peak strength, the concrete is expanded.
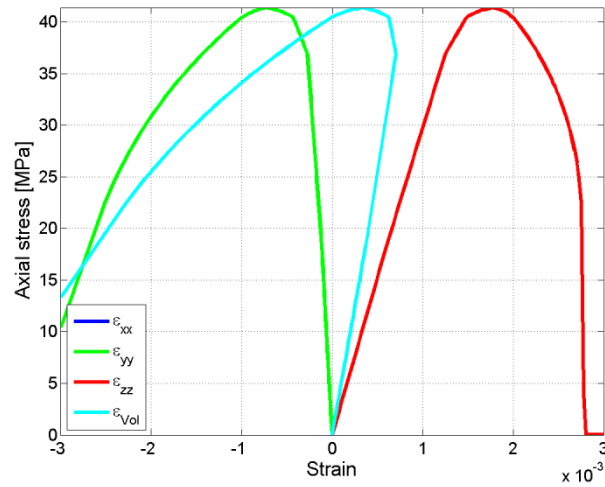
Figure 1 Single element UUC test

Figure 2 shows the stress – strain relationships for single element triaxial compression (TXC) tests, where solid line represents axial strain axial stress relationships, dotted lines represent lateral strain – axial stress relationships, and legend indicates confinement pressure.Several conclusions can be made from these tests. First, confinement effect is captured properly by the material model since concrete strength is observed much higher than its unconfined compressive strength (41.4 MPa). Second, the brittle – ductile transition under confinements is modeled properly. It is seen that strain softening behavior occurs when confinement pressure is low, and the concrete behaves elastic – hardening plastically, just like metal, when confinement pressure is very high.
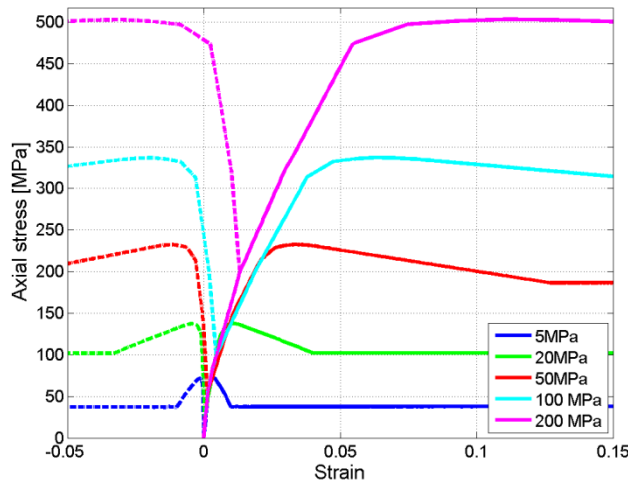

Figure 2 Single element TXC tests

Modified Cohesive Zone Model

In meshfree cohesive failure approach, a modified cohesive zone model [8] is utilized to describe the material failure of concrete in tension mode in addition to the concrete model described previously. The effective traction (T_{efs}) and the effective crack opening displacement (δ_{efs}) are defined as

$$T_{efs} = \sqrt{T_n^2 + \frac{1}{\beta^2}T_t^2} \text{, and} \tag{12}$$

$$\delta_{efs} = \sqrt{\delta_n^2 + \beta^2 \delta_t^2} \tag{13}$$

where the subscript n and t denote the normal and the tangential directions on the cracked surface (Γ_c) respectively as shown in Figure 3 and $\beta \geq 0$ is a parameter defined later.
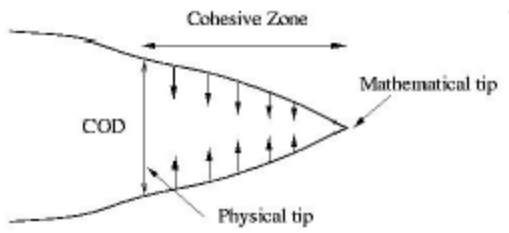

Figure 3 Cohesive zone model

The normalized non-dimensional displacement jump (Δ) and the critical displacement jump (Δ_c) [9] are introduced as

$$\Delta = \sqrt{\left(\frac{\delta_n}{\delta_{nf}}\right)^2 + \gamma^2\left(\frac{\delta_t}{\delta_{tf}}\right)^2} \text{, and} \tag{14}$$

$$\Delta_c = \sqrt{\left(\frac{\delta_{nc}}{\delta_{nf}}\right)^2 + \gamma^2\left(\frac{\delta_{tc}}{\delta_{tf}}\right)^2} \tag{15}$$

where the subscript c and f are the abbreviations of critical and failure respectively and $\gamma \geq 0$ is a parameter defined later. The failure opening displacement δ_{nf} and δ_{tf} are material constants, but the critical opening displacement δ_{nc} and δ_{tc} are numerically obtained by the visibility criterion when the crack is initiated as described previously. The initially-rigid irreversible cohesive can be assumed as

$$T_{efs}(\Delta) = \frac{1-\Delta^*}{1-\Delta_c}T_{max} \tag{16}$$

where T_{max} is the maximum tensile strength of a material and $\Delta^* = \max(\Delta_{max}, \Delta)$ which describes the irreversibility of the cohesive law. Then, the failure criterion is defined as

$$T_{efs}(\Delta) - T_{max} \geq 0 \tag{17}$$

which is the traction-driven failure criterion.

Originally, the initially-rigid cohesive law was proposed with the interface elements in the FE framework. In the FE framework, the crack initiation and propagation are occurred at nodes on the boundaries of elements. Hence, the critical opening displacement is always zero. However, in the meshfree method, the visibility criterion produces the positive non-zero critical opening displacement when the crack is initiated. Therefore, after the crack is initiated, the initially-elastic irreversible cohesive law with the critical opening displacement is adopted for the softening stage. This is the combined initially-rigid and initially-elastic irreversible cohesive law or the hybrid irreversible cohesive law. In other word, the initially-rigid cohesive law is used for the crack initiation and then it is switched to the initially-elastic irreversible cohesive law until the crack is separated completely. The initially-elastic irreversible cohesive laws of the normal and the tangential tractions can be defined as

$$T_n = \frac{T_{efs}(\Delta)}{\Delta^*} \frac{\delta_n}{\delta_{nf}} \qquad \text{, and} \tag{18}$$

$$T_t = \alpha \frac{T_{efs}(\Delta)}{\Delta^*} \frac{\delta_t}{\delta_{tf}} \tag{19}$$

where $\alpha \geq 0$ is a parameter defined later.

In the formulations above, there are three parameters, α, β and γ. The relationship among those parameters can be found. By inserting Eq. (18) and (19) into Eq. (16) at $t = t^c$, then Eq. (16) becomes

$$T_{efs} = \frac{T_{efs}(\Delta)}{\Delta_c} \sqrt{\left(\frac{\delta_{nc}}{\delta_{nf}}\right)^2 + \left(\frac{\alpha}{\beta}\right)^2 \left(\frac{\delta_{tc}}{\delta_{tf}}\right)^2}. \tag{20}$$

Obviously, the square root term in Eq. (20) should become Δ_c and is equal to Eq. (15). Then, we obtain

$$\gamma = \frac{\alpha}{\beta}. \tag{21}$$

By dividing Eq. (13) by δ_{nf}, then Eq. (13) becomes

$$\frac{\delta_{efs}}{\delta_{nf}} = \sqrt{\left(\frac{\delta_n}{\delta_{nf}}\right)^2 + \beta^2 \left(\frac{\delta_{tf}}{\delta_{nf}}\right)^2 \left(\frac{\delta_t}{\delta_{tf}}\right)^2}. \tag{22}$$

Let $\Delta = \dfrac{\delta_{efs}}{\delta_{nf}}$, using Eq. (14) and Eq. (21), we have

$$\alpha = \beta^2 \left(\frac{\delta_{tf}}{\delta_{nf}} \right). \tag{23}$$

Numerical Example

 A reinforced concrete structure under impact loading is analyzed with using meshfree cohesive failure approach. As in figure 3(a) and (b), the impactor is modeled such that the mass and strength distribution in the impact direction are corresponded to that of the scaled aircraft model. The thickness of RC panel is 6 cm, and the outer layer of panel is fixed. Reinforcement ration is 0.47% with D3 rebar. The concrete compressive strength is 31.4 N/mm^2. The common nodes are used to model the rebar coupled to the concrete. In case of cohesive failure, only mode I failure is considered. The maximum tensile strength T_{max} is taken to be 2.9 MPa and the critical displacement jump (Δ_c) is given by 0.01 mm in the analysis.

The final shapes of concrete plate in failure are plotted in Figures 4, 5 and 6 for FEM, EFG and cohesive failure approach respectively. As shown in Figure 4 (a), the failure shape of FEM concrete plate is close to a rectangle which is not an ideal circular shape. This is because the FEM mesh in concrete plate is originally discretized as a structured mesh. As a result, the elements in FEM are eroded depending on the orientation of the mesh. Compared to the FEM result, the final failure shape in EFG result using generalized meshfree approximation is closer to the ideal circular shape. Since EFG concrete plate requires less energy to create the material failure in circular shape, the residual velocity is higher than that in FEM method as shown in Table II. Both FEM and EFG with erosion approach generate similar amount of erosion in impactor as depict in Figure 3 (b) and 4 (b). The size of impactor radius in final shape is clearly smaller than the original radius due the material erosion in impactor. On the other hand, the impactor in meshfree cohesive failure approach retains the same size of radius during the penetration and creates a hole in concrete plate larger than the erosion approach. Because of that, the meshfree cohesive failure approach presents less residual speed than two erosion approaches which is closer to the reference solution in this study.
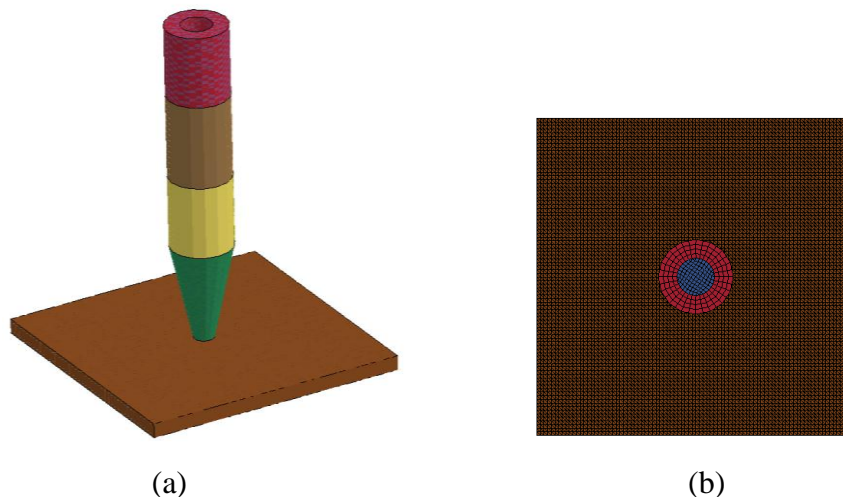

(a)   (b)

Figure 3. (a) Impact model. (b) Upper view of the model.

(a)   (b)
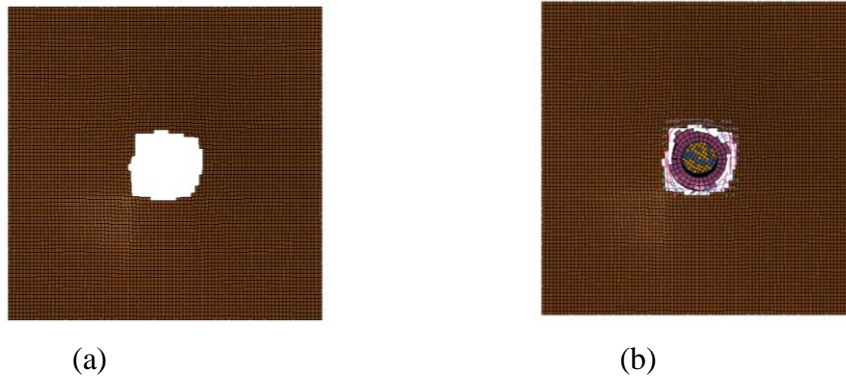
Figure 4. FEM with erosion: (a) Final failure shape of concrete. (b) Failure shape with impactor

(a)   (b)
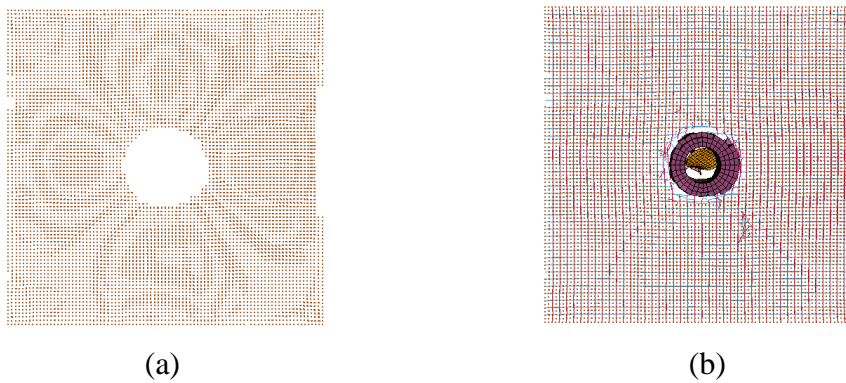
Figure 5. EFG with erosion: (a) Final failure shape of concrete. (b) Failure shape with impactor.

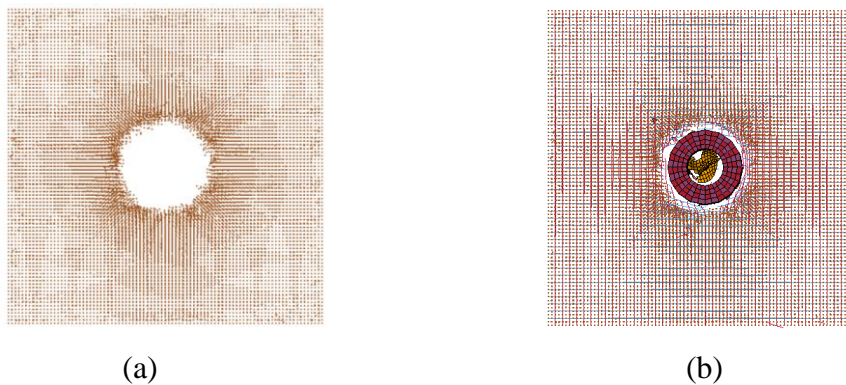(a)   (b)

Figure 6. Cohesive EFG: (a) Final failure shape of concrete. (b) Failure shape with impactor.

Table II. Residual velocity of impactor

	FEM + erosion	EFG + erosion	Cohesive EFG
velocity	103.5	112.4	94.5
Reference	80 (m/s)		

Conclusions

A simulation of reinforced concrete plate under impact loading using the meshfree cohesive failure approach is presented. The result is compared with two erosion approaches using FEM and EFG methods. Our numerical study reveals that FEM result is sensitive to the mesh orientation in which the final failure shape created by the impactor is depending on the generated mesh in the original model. In comparison to the FEM, two meshfree methods produce a failure shape in concrete plate that is more close to the ideal circular shape. The meshfree cohesive failure approach presents the lower residual speed and create large penetration hole comparing to the erosion approach. Although the meshfree cohesive failure approach utilizes the cohesive model to simulate the crack initiation and propagation in concrete material, it still relies on an erosion technique to handle the self-contact during the penetration. A study using cohesive meshfree-enriched finite element method [10] that incorporated tied node approach will be considered for this purpose in the next research phase.

Reference

[1] Wu, C. T., Park, C. K. and Chen, J.S. (2011), "A Generalized Approximation for the Meshfree Analysis of Solids" International Journal for Numerical Methods in Engineering, Vol. 85, pp.693-722.

[2] Rabczuk, T., Belytschko, T. (2007), "A three-dimensional large deformation meshfree method for arbitrary evolving cracks", Computer Methods in Applied Mechanics and Engineering, Vol. 196, pp.2777-2700.

[3] Chen, J. S., Wu, C. T., Yoon, S. and You, Y. (2001), "A Stabilized Confirming Nodal Integration for Galerkin Meshfree Methods," International Journal for Numerical Methods in Engineering, Vol. 53, pp. 2587-2615.

[4] Lu, H., Wu, C. T. (2010) "An Improved 3D Adaptive EFG Method for Forging and Extrusion Analysis with Thermal Coupling in LS-DYNA",11th International LS-DYNA Users Conference, Dearborn, Michigan, USA, June 6-8 2010.

[5] Crawford, J.E., Malvar, L.J., Valancius, J., Bogosian, D.D., Dunn, B.W., "Nonlinear Analysis for Seismic Upgrade Studies of Existing Essential Facilities," Computers and Structures, vol. 64, no. 5/6, June 1997, pp. 1183-1196.

[6] Crawford, J.E., Malvar, L.J., Wesevich. J.W., Valancius, J., Reynolds, A.D., "Retrofit of Reinforced Concrete Structures to Resist Blast Effects," ACI Structural Journal, vol. 94, no. 4, July-August 1997, pp. 371-377.

[7] Crawford, J.E., Magallanes, J.M., Lan, S., and Wu, Y. "User's manual and documentation for release III of the K&C concrete material model in LS-DYNA," TR-11-36-1, technical report, Karagozian& Case, Burbank, CA, November, 2011.

[8] Park, C. K. (2009) The development of a generalized meshfree approximation for solid and fracture analysis, Dissertation, The George Washington University.

[9] Espinosa, H.D. (2003) "A grain level model for the study of failure initation and evolution in polycrystalline materials. Part I: Theory and numerical implementation", Mechanics of Materials, vol. 35, no. 3-6, pp. 336-364.

[10] Wu C. T. and Hu, W. (2011), "Meshfree-enriched simplex elements with strain smoothing for the finite element analysis of compressible and nearly incompressible solids", Computer Methods in Applied Mechanics and Engineering, vol. 200, pp. 2991-3010.